AAEC/E 145
COPY NO. 80

AAEC/E 145

AUSTRALIAN ATOMIC ENERGY COMMISSION
RESEARCH ESTABLISHMENT
LUCAS HEIGHTS

BUCKLING AND INTEGRAL SPECTRUM MEASUREMENTS IN U233/BeO SUB-CRITICAL ASSEMBLIES

by

E. BRITTLIFF
P. DUERDEN

Issued Sydney, November 1965

OFFICIAL USE ONLY

AUSTRALIAN ATOMIC ENERGY COMMISSION

RESEARCH ESTABLISHMENT

LUCAS HEIGHTS

BUCKLING AND INTEGRAL SPECTRUM MEASUREMENTS IN U233/BeO SUB-CRITICAL ASSEMBLIES

by

E. BRITTLIFF

P. DUERDEN

ABSTRACT

The materials buckling of three BeO moderated U233 oxide fuelled systems having BeO/U233 ratios of 6496,4331, and 3248 have been measured by the exponential method. Relative fission rates of U233, U235, and Pu239 were also measured in the equilibrium spectrum region of the same assemblies. Because of the heterogeneous nature of the assembly, fine structure corrections have been applied. Some calculations using the CRAM Diffusion Code have been included.

CONTENTS

(continued)

CONTENTS (continued)

1. INTRODUCTION

As a further step in the study of beryllium oxide moderated reactor systems, buckling and fission rate measurements have been made with U233/BeO systems. Similar work on U235/BeO and U235/BeO/fertile material has been previously reported (Duerden et al. 1964; McCulloch et al. 1965).

2. MATERIALS

One kilogram of uranium–233 in the form of the oxides (UO_2, U_3O_8, etc.) was made available by the United States Atomic Energy Commission. These oxides, containing about 50 parts per million of the U232 isotope, were mixed with aluminium powder and cold pressed in wafers 0.020 in thick, each containing about one gram of uranium–233. Five such wafers were then sheathed in a 0.010 in thick aluminium can giving a fuel plate 11.85 in long by 1.34 in wide with an average U233 content of 4.851 grams.

The beryllium oxide and measurement of its diffusion properties for thermal neutrons have been described by Brittliff et al. (1963). 99.95 per cent. pure aluminium lattice plates 24in x 18in x 0.080in with slots 1.4in wide by 0.050in on a two–inch pitch were used to retain the fuel plates in the required configuration.

3. EXPERIMENTAL ARRANGEMENT

The three lattices in which measurements were made had the following BeO/U233 atomic ratios:

Lattice I	6496
Lattice II	4331
Lattice III	3248

The stack was approximately 18in x 19.5in x 24in high with the fuel plates vertically oriented, that is perpendicular to the source plane. It consisted of alternate layers of BeO tiles and slotted aluminium plates. Typical sections of the lattices are shown in Figures 1, 2, and 3, and the positions of the measuring holes are indicated in Figure 4.

The exact composition of each lattice is listed in Appendix 1.

4. MEASUREMENT OF THE MATERIALS BUCKLING

As in previously reported work, horizontal and vertical flux distributions in the stack were measured using ¼–inch diameter BF_3 proportional counters. All counts were taken with reference to a preset number of pulses from a one–inch diameter U235 fission counter fixed firmly in the reactor shield tank water at a position giving 800,000 pulses a minute at a reactor power of 5 kW. Flux scanning was thus rendered independent of drift in reactor power level. Horizontal measurements were made at 1 inch intervals to within 4 inches of the stack boundary. Vertical measurements were made at 1 inch intervals to within 14 inches of the top.

Noise and gain checks were made for each counting channel before commencing each day's runs. Checks were also made for the presence of spurious counts at the operating settings, and to ensure that bias characteristics of the channels had not deteriorated. In addition, the counter was returned to a fixed monitor position in the stack at frequent intervals. The aim was to achieve an overall accuracy of ± ½ per cent. or better on the flux measurement at any position.

4.1 Relaxation Lengths

Vertical scans were made in three positions, cadmium ratio measurements again being taken. In addition, further vertical scans were made with a ¼–inch thick sheet of boral placed between the top of the reactor and the graphite plinth. By subtraction it was then possible to obtain the vertical

flux distribution due to the required source below the stack alone, unperturbed by contribution from any in-leakage of fast neutrons through the sides and top of the assembly or from γ-n neutrons produced by direct gamma radiation from the reactor core and from the fuel plates themselves.

4.1.1 Errors

The error treatment has been described by McCulloch et al. (1965). A combination of the sources of error gives a total error of ± 0.56 per cent. for fluxes in vertical scans.

4.2 Extrapolated Widths

Horizontal scans were made at three different heights in the east-west direction and two in the north-south direction. Measurements were also made with the counter cadmium-covered to ensure that only measurements made in the region of equilibrium spectrum were included in the final analysis.

4.2.1 Errors

A combination of the sources of error gives a total error of ± 0.5 per cent. (see Section 4.1.1).

4.3 Results

Measured flux distributions are given in Appendices 2 to 4. Positional co-ordinates x,y are given in terms of distance from the east and north faces of the assembly; z co-ordinates are measured from the top of the graphite plinth.

4.3.1 Cadmium ratio measurements

Boron cadmium ratios were measured along each direction of the lattices and confirmed the existence of a constant cadmium ratio region in the lattices. The position of this region in the stack alters from lattice to lattice, as can be seen from the cadmium ratio plots shown in Figures 6, 7, and 8.

4.3.2 Relaxation lengths

Vertical flux distributions were fitted by the method of least squares to the function:

$$\phi = A \sinh \frac{h-z}{b_{11}} ,$$

where ϕ is the flux at height z,

h is the extrapolated height,

A is an amplitude coefficient, and

b_{11} is the relaxation length.

The position of the constant cadmium ratio region was checked by using different selections of measuring positions in the region. Relaxation lengths and extrapolated heights so derived are given in Table 1.

Examination of the table for trends in the data shows:

(i) There is no significant change of the relaxation length or the extrapolated height as the outermost points are omitted from the distribution. The relaxation length and extrapolated height calculated for the largest range was therefore used in all further calculations.

(ii) There is no significant difference between the values of the relaxation length or the extrapolated height calculated in the three vertical holes.

(iii) There is no significant difference between the values of the extrapolated height measured for a lattice and the weighted mean of the extrapolated height for all the lattices. The mean relaxation lengths and extrapolated heights are shown in Table 2.

4.3.3 N–S widths (y–widths)

No fine structure corrections were found to be necessary in this case since the scanning positions were at right angles to the fuel plates, and relatively remote from them. The fluxes were fitted, by weighted least squares, to the function:

$$\phi = A \cos \frac{\pi}{a_y}(y-\bar{y}) \quad .$$

The results are summarised in Table 3. Examination of this table for trends in the data shows:

(i) There is no significant change of the extrapolated width as the outermost points are omitted from the distribution, the ratio being:

$$\frac{a_y\ (x=5in \text{ to } 13in)}{a_y\ (x=4in \text{ to } 14in)} = 1.0043 \pm 0.0041 \quad .$$

(ii) There is no significant systematic trend of the extrapolated width from lattice to lattice, the ratios being:

$$\frac{a_y(II)}{a_y(I)} = 1.0000 \pm 0.0051, \quad \frac{a_y(III)}{a_y(I)} = 0.9996 \pm 0.0047 \quad .$$

(iii) There is a significant difference between the extrapolated widths measured at the two different heights in the stack, the ratio being:

$$\frac{a_y(z=45.30cm)}{a_y(z=30.06cm)} = 0.9912 \pm 0.0039 \quad .$$

Because a third harmonic component could be present in the distribution, the flux distributions for the range x = 4in to 14 in were fitted to the function:

$$\phi = A \cos \frac{\pi(y-\bar{y})}{a_y} + B \cos \frac{3\pi(y-\bar{y})}{a_y} \quad .$$

The results are given in Table 4. It can be seen that the limited range over which flux measurements were made again limits the accuracy of the results but the third harmonic content appears to be small and the mean calculated extrapolated width is similar to that obtained for the fundamental fit (53.50 ± 0.80 cm compared with 53.37 ± 0.11 cm).

The mean fundamental width was therefore adopted for the extrapolated width measurement but with an increased error of ± 0.20 cm which covers the possibility that either the top or bottom mean value could be representative of the true extrapolated N–S width of the stack.

4.3.4 E–W widths (x–widths)

The measurements were made at one–inch intervals to within four inches of the stack boundaries, cadmium ratio measurements indicating that this region was of adequately constant spectrum.

Owing to the heterogeneous nature of the lattices, fine structure corrections were necessary before the measured fluxes were fitted to a cosine distribution. Each correction was based on a one-dimensional slab cell calculation. The code used, FORTRAN DSN, was a translation of DSN (Carlson et al. 1960) in FORTRAN language (Clancy et al. 1965). It was necessary to represent a unit cell of the particular lattice in one-dimensional slab geometry. The appropriate one-dimensional cells of each lattice are shown in Figure 5. The code gives the relative fluxes along an axis of the cell when the cell is considered as part of an infinite system. Boron reaction rates were calculated along the cell axis. The BF_3 counter used in the experiment was 2½in long and to obtain a figure to compare with the measured count rate it was necessary to integrate the calculated reaction rates over a distance 1¼in on each side of the measuring position. When this had been done and the appropriate correction factor applied to the measured fluxes, these corrected fluxes were fitted by weighted least squares to the function:

$$\phi = A \cos \frac{\pi}{a_x} (x - \bar{x}) \quad ,$$

where ϕ is the corrected flux,

A is an arbitrary constant,

a_x is the extrapolated E-W width of the assembly, and

$\bar{x}$ is the 'centre' of the cosine distribution.

The measured fluxes, correction factors, and corrected fluxes are tabulated in Appendices 2 to 4. The maximum correction factor applied was 3 ± 0.5 per cent. The overall error in the corrected flux was therefore ± 0.7 per cent.

This procedure was carried out for the complete measuring range x = 4in to x = 14in and also for the range x = 5in to x = 13in. The results are summarised in Table 5.

Examination of this table for trends in the data shows:

(i) The change of the extrapolated width as the outermost points are omitted from the distribution is indicated by the ratio:

$$\frac{a_x (x = 5\text{in to } 13\text{in})}{a_x (x = 4\text{in to } 14\text{in})} = 1.0098 \pm 0.0050 \quad .$$

This is not considered to be a significant change.

(ii) There is no systematic trend of the extrapolated width from lattice to lattice, the ratios being:

$$\frac{a_x(I)}{a_x(II)} = 0.9934 \pm 0.0057 , \quad \frac{a_x(III)}{a_x(IV)} = 1.0114 \pm 0.0059 \quad .$$

(iii) There is a significant systematic trend of the extrapolated width with the height in the stack at which it was measured, the ratios being:

$$\frac{a_x(z = 15.66\,\text{cm})}{a_x(z = 30.90\,\text{cm})} = 1.0093 \pm 0.0058 , \frac{a_x(z = 46.14)}{a_x(z = 30.90)} = 1.0151 \pm 0.0059 \quad .$$

Only small differences in spectrum, as indicated by boron cadmium ratio measurements, were observed between the middle and top scanning holes, and since no dependence of the extrapolated width on lattice composition was observed, it is unlikely that spectrum changes could account for the observed trend.

Since a third harmonic component could be present in the distribution, the flux distributions in the range x = 4in to 14in were least squares fitted to the function:

$$\phi = A \cos \frac{\pi(x - \bar{x})}{a_x} + B \cos \frac{3\pi(x - \bar{x})}{a_x} \quad .$$

The results are given in Table 6 and indicate the possible presence of a small harmonic component of comparable size to the fine structure correction factor applied to the measured fluxes. Because of this the mean width of 50.16cm, obtained by fitting to a fundamental function only, was used as the extrapolated E–W width, but with an increased error of ± 0.40cm similar to that adopted in the in the N–S case.

4.3.5 Stack dimensions

The overall dimensions for each stack were obtained by measuring each layer of tiles. The mean values are quoted in the footnote to Table 7.

4.3.6 Extrapolated distances

The extrapolated distances λ_x , λ_y , and λ_h for each of the measuring holes, as well as the appropriate means, are given in Table 7. It is seen that they form a consistent set with a weighted mean value of 1.96 ± 0.06 cm. This value for λ is not inconsistent with the values quoted for the softer lattices in Duerden et al. (1964); these lattices have a similar spectrum hardness to the current series of lattices.

4.3.7 The materials buckling

The buckling components calculated from the measured values of extrapolated widths and relaxation lengths for each lattice are given in Table 8.

Because of the heterogeneous nature of the stacks we may write:

$$K^2 = \frac{M_{//}^2}{M^2}\left[\left(\frac{\pi}{a_x}\right)^2 - \left(\frac{1}{b_{11}}\right)^2\right] + \frac{M_{\perp}^2}{M^2} \cdot \left(\frac{\pi}{a_y}\right)^2 ,$$

where K^2 is the materials buckling of an homogeneous lattice of the same composition as the experimental stack (neglecting the effects of fine–structure flux depressions),

M^2 is the migration area in the corresponding homogeneous lattice, and

$M_{//}^2$ and $M_{\perp}^2$ are the migration areas for the experimental lattice, respectively parallel and perpendicular to the slabs.

No satisfactory method for the calculation of $(M_{//}/M)^2$ or $(M_{\perp}/M)^2$ in slab geometry has been published and a two–orientation method measurement of $M_{//}^2/M_{\perp}^2$ would not be sufficiently accurate to be justifiable. This method involves turning the stack through 90° so that the source plane is now parallel to the fuel plates, and repeating the measurements of buckling. Keane (1965) has suggested a method for the calculation of $M_{//}^2/M_{\perp}^2$ in a case similar to ours, where there is a small gap containing a strongly absorbing media between layers of the moderator. We will assume without significant error that $M_{\perp}^2 = M^2$. Keane's method gives $M_{//}^2/M_{\perp}^2 = 1.021$ for Lattice I, 1.017 for Lattice II, and 1.008 for Lattice III. In no case does the correction to the materials buckling as calculated directly from the measured components exceed 0.2 of the experimental standard deviation. No corrections for asymmetry have therefore been included in the experimental materials buckling values given in Table 8.

5. INTEGRAL SPECTRUM MEASUREMENTS

Relative fission rates of U235, U233, and Pu239 using intercalibrated fission chambers were carried out as described by McCulloch et al. (1965), the only difference being that the chambers were positioned in vertical hole B (nearest the centre of the lattice), the insertion depth being chosen to ensure that measurements were made well within the region of constant spectrum.

5.1 Flux Depression due to Fission Chamber Wall

A measurement of the effect of the wall on each chamber was made in Lattice II, and the results obtained agreed very well with the values given in McCulloch et al.'s Figure 3. This was taken as sufficient justification to use the least squares fitted parameters quoted in that work.

5.2 Errors

The sources of error and their magnitudes are listed below. Unless otherwise stated, they are exactly the same as reported by McCulloch et al. (1965).

5.2.1 Random errors – thermal calibration

(a) Statistical counting errors – contribution to the uncertainty of each ratio of 0.46 per cent.

(b) Control channel statistics 0.2 per cent.

(c) Count channel gain drift 0.5 per cent.

(d) Control channel sensitivity drift 0.2 per cent.

(e) Counter positioning 0.1 per cent.

(f) Paralysis time 0.3 per cent.

(g) Total random error

Combination of the above gives the uncertainty of a single ratio as ± 0.8 per cent.

5.2.2 Random errors – lattice measurements

(a) Count channel statistics 0.7 per cent.

(b) Control channel statistics 0.1 per cent.

(c) Counter positioning

The counter was positioned in a vertical flux scanning hole with a maximum gradient of about 15 per cent. per inch. Positioning was accurate to 0.010in giving a maximum uncertainty of 0.25 per cent.

(d) Paralysis time 0.05 per cent.

(e) Total Random Error

Combining the above sources of error gives the uncertainty on a single ratio measurement in the lattices as ± 0.9 per cent.

5.2.3 Systematic errors

These are also identical with the systematic errors quoted by McCulloch et al. (1965) except for the effect of the uncertainty in the position of the active volume which gives rise in this case to an error of 0.25 per cent., since the counters are positioned in a vertical hole.

The errors due to the nickel and stainless steel wall corrections are ± 0.58 per cent, and ± 0.14 per cent. respectively for the thermal flux measurements. For the lattice measurements, the uncertainty in the effect of the stainless steel contributes 0.25 per cent. to the error, and the contribution of the uncertainty in the nickel wall correction ranges between 0.80 per cent. and 0.35 per cent., depending on spectrum hardness. The error on the available Maxwellian averaged cross section data (Westcott 1960) is ± 1 per cent.

5.2.4 Total error

Consideration of all the above sources of error gives an uncertainty in the fission ratio per fissile atom in the range 1.73 to 1.63 per cent.

5.3 Results

The fission ratios per fissile atom are given in Table 9 whilst the relative count rates as measured in the lattices and the thermal column are given in Appendix 5.

6. COMPARISON OF EXPERIMENTS WITH THEORY

Some calculations have been carried out using the multigroup diffusion theory code CRAM (Hassitt 1962) for a bare homogeneous spherical reactor system with the composition used in the assemblies.

The 18-group cross sections used for BeO, O, U233, U235, Al, and Pu239 are those listed by Bell et al. (1963), but have been modified as follows.

BeO Upscattering has been included, based upon data generated by PIXSE (McDougal 1963) using a tabulation of $S(\alpha\beta)$ (Sinclair 1962) obtained from LEAP (McLatchie 1962). This has been included by reducing the self-scattering term and maintaining σ_{tr} as the value given by Bell et al. (1963).

U233 The value of $\overline{\nu}$ used is that due to Smith (1964). Self-shielding factors for the resonance region were calculated on the basis of aluminium in the fuel plates being intimately mixed with the U_2O_3, and using curves given by Roach (1960). A value of σ_p = 60 barns was used. The cross sections used in Group 10 could be a source of error as Roach considers a group with boundaries 30 eV – 100 eV; our comparable group has boundaries 22.6 eV–61.44 eV.

U234 σ_c, σ_f used are those of Hughes (1958) transformed into multigroup form. $\Sigma_{i\rightarrow j}$ used are those pertaining to U233. No self-shielding factors have been included.

The cross sections used are listed in Appendix 6. The normalised neutron fluxes as a function of lethargy are shown in Figure 9.

The materials bucklings of the assemblies were calculated using the critical radii and the experimental value of the extrapolation distance. The calculated and experimental values of B_m^2 are shown in Figure 10. It can be seen that the calculated value is approximately 5 per cent. larger than the experimental value. This may be a shape factor effect, since otherwise the U233 cross sections used would appear to be too reactive. The presence of 2½ per cent. of U234 in the fuel is seen to decrease the materials buckling by about 1 per cent.

Fission ratios have been obtained using the calculated neutron fluxes at the centre of the critical system; the fluxes are listed in Appendix 7. Self-shielding of the fission cross sections in the resonance region was not considered, as the fissile material in the detectors is only of the order of 2×10^{-5} cm thick.

It can be seen from Figure 11 that good agreement between the calculated and experimental values of the U233/U235 ratio was obtained but that the calculated Pu239/U235 ratios are too high. It appears that some self-shielding of the fission cross section in the Pu239 resonance region must be considered.

The calculated and experimental results are compared in Table 10.

7. CONCLUSIONS

The materials bucklings of the three chosen BeO/U233 lattices have been measured to an accuracy of approximately ± 3 per cent. Relative fission ratios have been measured to approximately ± 2 per cent.

Some simple calculations have been carried out. The calculated materials bucklings were 5 per cent. larger than the experimental values; good agreement was obtained for the U233/U235 fission ratios but the calculated Pu239/U235 ratios were larger than the experimental ratios. Calculations are in progress to resolve these differences.

8. ACKNOWLEDGEMENTS

The authors would like to acknowledge the assistance of Mr. R. East, and the MOATA operations team. The assistance of Mr. T. Kaar in the preparation of the DSN programmes is also gratefully acknowledged.

9. REFERENCES

Bell, G.I., Devaney, J.J., Hansen, G.E., Mills, C.B., and Roach, W.H. (1963). – LAMS 2941.

Brittliff, E., Duerden, P., and McCulloch, D.B. (1963). – AAEC/TM203.

Carlson, B., Lee, C.J., and Worlton, J. (1960). – LAMS 2346.

Clancy, B., Scott, A., and Steps, M. (1965). – Unpublished A.A.E.C. Internal Report.

Duerden, P., McCulloch, D.B., and Brittliff, E. (1964). – AAEC/E123.

Hassitt, A. (1962). – TRG 229 (R).

Hughes, D.J., and Schwartz, R.B. (1958). – BNL 325.

Keane, A. (1965). – AAEC/TM 302

McCulloch, D.B., Duerden, P., and Brittliff, E. (1965). – AAEC/E report in preparation.

McDougal, J.D. (1963). – AEEW – M 318.

McLatchie, R.F.C. (1962). – UKAEA Internal Report.

Roach, W.H. (1960). – Nucl. Sci. and Engng. 8(6):621.

Smith, A.B. (1964). – ANL 6792.

Sinclair, R.N. (1962). – AERE NP.GEN 28.

Westcott, C.H. (1960). – AECL 1101.

TABLE 1

RELAXATION LENGTHS AND EXTRAPOLATED HEIGHTS

Lattice	Position Set	Hole A x = 15.65 cm y = 17.82 cm			Hole B x = 27.94 cm y = 26.94 cm			Hole C x = 30.07 cm y = 34.37 cm		
		$b_{//}$ (cm)	h (cm)	$\Sigma \frac{\delta^2}{\sigma^2}$	$b_{//}$ (cm)	h (cm)	$\Sigma \frac{\delta^2}{\sigma^2}$	$b_{//}$(cm)	h (cm)	$\Sigma \frac{\delta^2}{\sigma^2}$
I	A	15.58 ±0.40	62.86 ±0.56	3.7	15.85 ±0.42	62.19 ±0.48	5.3	15.81 ±0.42	62.28 ±0.49	1.6
	B	16.06 ±0.65	62.44 ±0.63	2.6	16.38 ±0.69	61.83 ±0.55	4.1	15.82 ±0.62	62.27 ±0.61	1.6
	C	15.71 ±0.62	62.57 ±1.08	3.6	15.53 ±0.59	62.84 ±1.14	4.8	16.22 ±0.68	61.58 ±0.88	0.9
	D	16.88 ±1.22	61.41 ±1.12	1.7	16.22 ±1.09	62.02 ±1.29	4.1	16.68 ±1.18	61.19 ±1.07	0.6
II	A	16.75 ±0.14	63.33 ±0.20	3.8	17.05 ±0.14	63.04 ±0.19	9.7	17.19 ±0.14	62.94 ±0.18	20.6
	B	16.77 ±0.16	63.31 ±0.24	3.7	17.00 ±0.17	63.08 ±0.20	9.4	17.17 ±0.17	62.96 ±0.20	20.6
	C	16.79 ±0.17	63.19 ±0.19	3.5	16.90 ±0.17	63.47 ±0.36	7.4	17.20 ±0.18	62.93 ±0.32	20.6
	D	16.85 ±0.21	63.12 ±0.37	3.4	16.77 ±0.21	63.64 ±0.41	6.3	17.17 ±0.22	62.97 ±0.36	20.6
III	A	18.94 ±0.19	62.99 ±0.18	8.4	19.30 ±0.20	62.86 ±0.17	18.8	19.00 ±0.19	63.02 ±0.18	19.5
	B	19.09 ±0.24	62.91 ±0.19	7.2	19.08 ±0.23	62.97 ±0.19	16.2	18.76 ±0.22	63.15 ±0.20	16.4
	C	18.93 ±0.23	63.00 ±0.31	8.4	19.46 ±0.23	62.60 ±0.28	17.6	19.11 ±0.24	62.82 ±0.30	18.8
	D	19.13 ±0.30	62.84 ±0.33	7.1	19.19 ±0.30	62.79 ±0.32	15.7	18.83 ±0.29	63.04 ±0.35	16.2

Set A includes measuring positions 4 – 10 for Lattice I and 3 – 14 for Lattices II and III

Set B " " " 4 – 9 " 3 – 13 " "

Set C " " " 5 – 10 " 4 – 14 " "

Set D " " " 5 – 9 " 4 – 14 " "

TABLE 2

MEAN RELAXATION LENGTHS AND EXTRAPOLATED HEIGHTS

Lattice	b_{II} (cm)	h (cm)
I	15.75 ±0.24	62.44 ±0.29
II	17.00 ±0.08	63.10 ±0.11
III	19.08 ±0.11	62.96 ±0.10

Weighted Mean of Extrapolated Heights = 62.99 ± 0.07

TABLE 3

EXTRAPOLATED y– WIDTHS

Lattice	Position		10.97 < y < 38.40		13.72 < y < 35.66	
	z = (cm)	x = (cm)	a_y	$\Sigma\frac{\delta^2}{\sigma^2}$	a_y	$\Sigma\frac{\delta^2}{\sigma^2}$
I	30.06	35.56	53.49 ±0.23	29.8	53.97 ±0.44	28.6
	45.30	20.32	53.26 ±0.23	36.4	53.54 ±0.43	35.3
II	30.06	35.56	53.72 ±0.27	6.1	54.02 ±0.50	4.5
	45.30	20.32	53.00 ±0.27	7.6	52.48 ±0.47	3.1
III	30.06	35.56	53.58 ±0.27	11.6	54.58 ±0.51	3.4
	45.30	20.32	53.13 ±0.26	3.4	52.95 ±0.48	1.7

TABLE 4

EXTRAPOLATED y–WIDTHS WITH 3RD HARMONIC COMPONENT

Lattice	Position		10.97 < y < 38.40			
	z = (cm)	x = (cm)	a_y	A	B	$\Sigma \frac{\delta^2}{\sigma^2}$
I	30.06	35.56	53.91 ±1.75	341 ±4.7	1.07 ±5.24	29.8
	45.30	20.32	53.54 ±1.25	162 ±1.6	0.42 ±1.9	31.5
II	30.06	35.56	51.61 ±1.46	8995 ±87	−145 ±101	4.5
	45.30	20.32	56.28 ±2.96	4607 ±101	115 ±109	5.7
III	30.06	35.56	50.27 ±1.22	9617 ±76	−248 ±92	6.7
	45.30	20.32	55.42 ±2.50	5062 ±92	88 ±100	2.3

TABLE 5

EXTRAPOLATED x – WIDTHS

Lattice	Position		10.16 < x < 35.56		12.70 < x < 33.02	
	z = (cm)	y = (cm)	a_x	$\Sigma \frac{\delta^2}{\sigma^2}$	a_x	$\Sigma \frac{\delta^2}{\sigma^2}$
I	15.66	31.61	49.60 ±0.32	7.7	50.45 ±0.63	5.3
	30.90	23.33	49.89 ±0.36	1.0	50.25 ±0.67	0.6
	46.14	15.06	50.74 ±0.38	11.2	52.61 ±0.76	1.6
II	15.66	31.61	50.63 ±0.35	12.1	50.76 ±0.63	7.3
	30.90	23.33	48.78 ±0.32	14.7	48.11 ±0.56	13.0
	46.14	15.06	49.85 ±0.34	15.7	49.93 ±0.62	15.7
III	15.66	31.61	50.50 ±0.38	10.3	51.55 ±0.73	6.1
	30.90	23.33	50.46 ±0.38	4.2	50.68 ±0.70	3.9
	46.14	15.06	51.00 ±0.38	7.4	51.55 ±0.71	4.5

TABLE 6

EXTRAPOLATED x – WIDTHS WITH 3RD HARMONIC COMPONENTS

Lattice	Position		$10.16 < x < 35.56$			
	z = (cm)	y = (cm)	a_x	A	B	$\Sigma \frac{\delta^2}{\sigma^2}$
I	15.66	31.61	45.31 ±1.30	32483 ±197	−1449 ±247	2.1
	30.90	23.33	48.44 ±2.16	12380 ±132	− 146 ±152	0.7
	46.14	15.06	45.66 ±1.33	10417 ±72	− 348 ±88	2.9
II	15.66	31.61	54.08 ±4.65	20017 ±567	685 ±600	15.8
	30.90	23.33	60.42 ±10.40	7688 ±846	757 ±853	8.3
	46.14	15.06	51.23 ±2.81	2491 ±38	5.3 ± 42	12.9
III	15.66	31.61	47.74 ±1.85	28163 ±247	− 726 ±292	5.4
	30.90	23.33	49.83 ±2.56	12831 ±165	− 66 ±186	4.2
	46.14	15.06	47.58 ±1.84	4262 ±37	− 101 ±44	8.6

TABLE 7

EXTRAPOLATED DISTANCES

Lattice		I	II	III
E–W 6in level	λ_x	1.86 ±0.12	2.38 ±0.13	2.31 ±0.13
E–W 12in level	λ_x	2.01 ±0.14	1.45 ±0.12	2.29 ±0.14
E–W 18in level	λ_x	2.43 ±0.14	1.99 ±0.12	2.56 ±0.14
N–S 12in level	λ_y	2.03 ±0.12	2.15 ±0.14	2.08 ±0.13
N–S 18in level	λ_y	1.92 ± 0.12	1.79 ±0.14	1.85 ±0.13
Vertical HoleA	λ_h	1.23 ±0.49	1.89 ±0.18	1.97 ±0.18
Vertical Hole B	λ_h	1.04 ±0.48	1.99 ±0.19	1.81 ±0.17
Vertical Hole C	λ_h	1.81 ±0.56	2.28 ±0.20	1.94 ±0.18

Mean E–W	λ_x	1.94 ±0.07
Mean N–S	λ_y	2.14 ±0.21
Mean Vertical	λ_h	1.97 ±0.13

The measured stack dimensions are: E – W (a_x) phys. = 45.88 ± 0.10 cm
N – S (a_y) phys. = 49.43 ± 0.15 cm
Height (h) phys. = 61.05 ± 0.05 cm

TABLE 8

THE MATERIALS BUCKLING

Lattice	$(\pi/a_x)^2$ (m^{-2})	$(\pi/a_y)^2$ (m^{-2})	$\left(\frac{1}{b_{II}}\right)^2$ (m^{-2})	K^2 (m^{-2})
I	39.23 ±0.63	34.65 ±0.26	40.31 ±1.23	33.6 ±1.4
II	39.23 ±0.63	34.65 ±0.26	34.60 ±0.33	39.3 ±0.8
III	39.23 ±0.63	34.65 ±0.26	27.47 ±0.32	46.4 ±0.8

TABLE 9

MEASURED FISSION RATIOS

Lattice	Fission Ratio per Fissile Atom	
	Pu239/U235	U233/U235
I	1.608 ±0.027	1.003 ±0.017
II	1.761 ±0.030	1.079 ±0.018
III	1.777 ±0.030	1.081 ±0.018

TABLE 10

COMPARISON OF EXPERIMENTAL RESULTS AND CALCULATIONS

Materials Buckling (m^{-2})

Lattice	Expt.	Calc.	Calc. (No U234)
I	33.6 ±1.4	33.48	33.74
II	39.3 ±0.8	42.58	42.90
III	46.4 ±0.8	48.87	49.24

Fission Ratios

Lattice	Pu239/U235		U233/U235	
	Expt.	Calc. $\sigma_p = \infty$	Expt.	Calc. $\sigma_p = \infty$
I	1.608 ±0.027	2.103	1.003 ±0.017	1.061
II	1.761 ±0.030	2.010	1.079 ±0.018	1.095
III	1.777 ±0.030	1.899	1.081 ±0.018	1.127

APPENDIX 1

LATTICE MATERIALS

(a) Composition of Homogeneously Smeared Experimental Lattices in atoms/cm^3

Element	III	II	I
Be	6.4049×10^{22}	6.4049×10^{22}	6.4049×10^{22}
O	6.4089×10^{22}	6.4089×10^{22}	6.4089×10^{22}
Al	3.3823×10^{21}	3.1633×10^{21}	2.9443×10^{21}
U233	1.9688×10^{19}	1.4766×10^{19}	9.8442×10^{18}
U234	4.780×10^{17}	3.585×10^{17}	2.390×10^{17}
U235	4.25×10^{16}	3.19×10^{16}	2.13×10^{16}
U236	3.2×10^{15}	2.4×10^{15}	1.6×10^{15}
U238	5.09×10^{16}	3.82×10^{16}	2.54×10^{16}

(b) Mean Fuel Strip Data

Dimension: 11.86in x 1.341in x 0.042in

Composition: Aluminium 24.93 g

Uranium 4.851 g

U232 concentration 50 parts per million.

(c) Aluminium Lattice Plates

Material: 99.95 per cent. pure aluminium

Dimensions: 24in x 18in x 0.080in

Weight: 860 g.

APPENDIX 2

LATTICE I FLUX MEASUREMENTS

(a) E–W (x) Widths

x (cm)	z = 15.66 cm y = 31.61 cm			z = 30.90 cm y = 23.33 cm			z = 46.14 cm y = 15.06 cm		
	Observed Flux	Fine Structure Correction Factor	Corrected Flux	Observed Flux	Fine Structure Correction Factor	Corrected Flux	Observed Flux	Fine Structure Correction Factor	Corrected Flux
10.16	21814	1.0081	21991	8675	0.9846	8541	7145	0.9846	7035
12.70	25696	1.0000	25696	10112	0.9743	9856	8357	0.9743	8146
15.24	28624	0.9846	28183	11065	0.9846	10895	9245	0.9846	9103
17.78	30628	0.9747	29853	11666	1.0000	11666	9680	1.0000	9680
20.32	31333	0.9846	30850	12006	1.0081	12103	9880	1.0081	9960
22.86	30924	1.0000	30924	12230	1.0000	12230	10060	1.0000	10060
25.40	30543	1.0081	30790	12281	0.9846	12092	10051	0.9846	9896
27.94	29626	1.0000	29626	11873	0.9747	11573	9859	0.9747	9610
30.48	28357	0.9846	27920	11046	0.9846	10876	9136	0.9846	8995
33.02	26023	0.9747	25365	9848	1.0000	9848	8078	1.0000	8078
35.56	22239	0.9846	21897	8441	1.0081	8509	6904	1.0081	6960

Fluxes are in arbitrary units

(continued)

APPENDIX 2 (continued)

(b) N – S Widths

y (cm)	Observed Flux	
	z = 30.06 cm x = 35.56 cm	z = 45.30 cm y = 20.32 cm
10.97	2320	1115
13.72	2708	1305
16.46	3009	1435
19.20	3183	1534
21.95	3368	1634
24.69	3430	1666
27.43	3429	1652
30.18	3210	1549
32.92	3031	1492
35.66	2790	1343
38.40	2408	1163

(c) Relaxation Lengths

z (cm)	Observed Flux		
	x = 30.07 cm y = 34.37 cm	x = 27.94 cm y = 26.94 cm	z = 15.65 cm y = 17.82 cm
50.90	1523	1561	1377
48.36	1929	1993	1742
45.82	2408	2504	2150
43.28	2934	3004	2647
40.74	3557	3635	3175
38.20	4224	4358	3768
35.66	5045	5216	4540

Units of flux are arbitrary

APPENDIX 3

LATTICE II FLUX MEASUREMENTS

(a) E – W (x) Widths

x (cm)	Fine Structure Correction Factor	z = 15.66 cm y = 31.61 cm		z = 30.90 cm y = 23.33 cm		z = 46.14 cm y = 15.06 cm	
		Observed Flux	Corrected Flux	Observed Flux	Corrected Flux	Observed Flux	Corrected Flux
10.16	1.0000	14426	14426	5806	5806	1767	1767
12.70	0.9754	17030	16611	6894	6725	2115	2063
15.24	1.0000	18278	18278	7393	7393	2226	2226
17.78	1.0252	19152	19634	7680	7873	2325	2384
20.32	1.0000	20284	20284	8271	8271	2445	2445
22.86	0.9754	21444	20917	8734	8519	2577	2514
25.40	1.0000	20509	20509	8394	8394	2483	2483
27.94	1.0252	18984	19462	7729	7924	2290	2348
30.48	1.0000	17908	17908	7311	7311	2206	2206
33.02	0.9754	17134	16713	6771	6605	2057	2006
35.56	1.0000	14300	14300	5720	5720	1764	1764

Units of flux are arbitrary

(continued)

APPENDIX 3 (continued)

(b) N – S (y) Widths

y (cm)	Observed Flux	
	z = 30.06 cm x = 35.56	z = 45.30 cm y = 20.32 cm
10.97	6095	3188
13.72	7091	3672
16.46	7868	4111
19.20	8418	4407
21.95	8685	4620
24.69	8844	4719
27.43	8781	4673
30,18	8437	4522
32.92	7928	4217
35.66	7116	3791
38.40	6225	3300

(c) Relaxation Lengths

z (cm)	Observed Flux		
	x = 30.07 cm y = 34.37 cm	x = 27.94 cm y = 26,94 cm	x = 15.65 cm y = 17.82 cm
53.44	1084	1145	1023
50.90	1422	1519	1320
48.36	1780	1875	1673
45.82	2160	2305	2025
43.28	2595	2770	2457
40.74	3141	3325	2941
38.20	3735	3933	3483
35.66	4396	4648	4096
33.12	5194	5438	4842
30.58	5986	6423	5636
28.04	6888	7395	6611
25.50	8114	8635	7741

Units of flux are arbitrary

APPENDIX 4

LATTICE III FLUX MEASUREMENTS

(a) E – W Flux Scans

x (cm)	Fine Structure Correction Factor	z = 15.66 cm y = 31.61 cm		z = 30.90 cm y = 23.33 cm		z = 46.14 cm y = 15.06 cm	
		Observed Flux	Corrected Flux	Observed Flux	Corrected Flux	Observed Flux	Corrected Flux
10.16	1.0000	19694	19694	8952	8952	2907	2907
12.70	0.9681	23131	22393	10674	10333	3486	3375
15.24	0.9612	25762	24762	11801	11343	3905	3753
17.78	0.9681	26882	26024	12471	12073	4092	3961
20.32	1.0000	27263	27263	12673	12673	4128	4128
22.86	1.0125	26945	27282	12669	12827	4126	4178
25.40	1.0000	27215	27215	12563	12563	4124	4124
27.94	0.9681	27144	26278	12465	12067	4057	3928
30.48	0.9612	25728	24730	11923	11460	3846	3697
33.02	0.9681	22996	22262	10636	10297	3528	3415
35.56	1.0000	19292	19292	9001	9001	2947	2947

Fluxes are in arbitrary units

(continued)

APPENDIX 4 (continued)

(b) N – S Widths

y (cm)	Observed Flux	
	z = 30.06 cm x = 35.56 cm	z = 45.30 cm x = 20.32 cm
10.97	6438	3457
13.72	7474	4008
16.46	8301	4462
19.20	8845	4810
21.95	9203	5067
24.69	9368	5155
27.43	9297	5089
30,18	9029	4919
32.92	8428	4601
35.66	7654	4184
38.40	6563	3628

(c) Relaxation Lengths

z (cm)	Observed Flux		
	x = 30.07 cm y = 34.37 cm	x = 27.94 cm y = 26.94 cm	x = 15.65 cm y = 17.82 cm
53.44	1528	1658	1338
50.90	1987	2147	1740
48.36	2450	2673	2165
45.82	2970	3260	2629
43.28	3565	3854	3147
40.74	4219	4617	3715
38.20	5011	5397	4404
35.66	5810	6265	5128
33.12	6805	7364	5846
30.58	7732	8454	6816
28.04	8858	9524	7805
25.50	10165	10965	9081

APPENDIX 5

RELATIVE FISSION RATES IN THE LATTICES

	U235	U233	Pu239
Lattice I	1.000 ± 0.009	0.317 ± 0.003	0.146 ± 0.001
Lattice II	1.000 ± 0.009	0.341 ± 0.003	0.160 ± 0.002
Lattice III	1.000 ± 0.009	0.342 ± 0.003	0.161 ± 0.002
Thermal Column	1.000 ± 0.006	0.295 ± 0.002	0.126 ± 0.001
* Relative Effective Number of Atoms	1.000 ± 0.012	0.316 ± 0.004	0.0908 ± 0.0011

* Relative effective number of fissile atoms was calculated using effective 20.44 ° C Maxwellian averaged cross sections given by Westcott (1960), namely:

$$\sigma_{f5} = 563.1 \text{ b}$$

$$\sigma_{f3} = 525.2 \text{ b}$$

$$\sigma_{f9} = 778.3 \text{ b}$$

APPENDIX 6

18 – GROUP CROSS SECTIONS

(a) 18–Group Cross Sections used in CRAM Calculation

BeO

Group	σ_{tr}	σ_{rem}	$\sigma_{g\to g-3}$	$\sigma_{g\to g-2}$	$\sigma_{g\to g-1}$	$\sigma_{g\to g+1}$	$\sigma_{g\to g+2}$	$\sigma_{g\to g+3}$	$\sigma_{g\to g+4}$
1	2.172	1.324	–	–	–	1.242	0.35	0.0	0.0
2	2.455	0.732	–	–	0.0	0.7	0.12	0.0	0.0
3	5.61	2.109	–	0.0	0.0	2.109	0.0	0.0	0.0
4	6.94	1.815	0.0	0.0	0.0	1.815	0.0	0.0	0.0
5	7.65	0.971	0.0	0.0	0.0	0.971	0.0	0.0	0.0
6	8.44	0.881	0.0	0.0	0.0	0.881	0.0	0.0	0.0
7	8.83	0.935	0.0	0.0	0.0	0.935	0.0	0.0	0.0
8	9.01	1.06	0.0	0.0	0.0	1.06	0.0	0.0	0.0
9	9.06	1.06	0.0	0.0	0.0	1.06	0.0	0.0	0.0
10	9.10	1.68	0.0	0.0	0.0	1.68	0.0	0.0	0.0
11	9.10	1.6803	0.0	0.0	0.0	1.68	0.0	0.0	0.0
12	9.10	1.6804	0.0	0.0	0.0	1.68	0.0	0.0	0.0
13	9.10	1.6807	0.0	0.0	0.0	1.68	0.0	0.0	0.0
14	9.10	1.4985	0.0	0.0	0.0	1.4795	0.0171	0.0006	0.0001
15	9.10	1.1342	0.0	0.0	0.0581	1.013	0.0527	0.0085	–
16	9.10	0.604	0.0	0.0	0.1567	0.3298	0.1123	–	–
17	9.00	0.3951	0.0	0.0065	0.2869	0.0933	–	–	–
18	8.306	0.3126	0.0014	0.1614	0.1406	–	–	–	–

U233 σ_p = 60

Group	σ_{tr}	σ_{rem}	$\nu\sigma_f$	$\sigma_{g\to g+1}$	$\sigma_{g\to g+2}$	$\sigma_{g\to g+3}$	$\sigma_{g\to g+4}$	$\sigma_{g\to g+5}$
1	4.25	3.07	5.64	0.20	0.27	0.45	0.31	0.04
2	4.5	2.99	5.08	0.18	0.50	0.35	0.05	0.0
3	4.8	2.81	4.94	0.45	0.30	0.06	0.0	0.0
4	5.7	2.43	4.93	0.29	0.05	0.0	0.0	0.0
5	8.4	2.52	5.56	0.05	0.0	0.0	0.0	0.0
6	12.0	3.83	7.93	0.05	0.0	0.0	0.0	0.0
7	16.82	6.82	14.6	0.05	0.0	0.0	0.0	0.0
8	20.25	10.25	21.9	0.05	0.0	0.0	0.0	0.0
9	37.45	27.45	58.4	0.05	0.0	0.0	0.0	0.0
10	57.35	47.35	70.4	0.05	0.0	0.0	0.0	0.0
11	93.65	83.65	175.6	0.05	0.0	0.0	0.0	0.0
12	100.95	90.95	188.2	0.05	0.0	0.0	0.0	0.0
13	258.55	248.55	484.6	0.05	0.0	0.0	0.0	0.0
14	171.0	161.0	321.5	0.05	0.0	0.0	0.0	–
15	214.8	204.85	446.2	0.05	0.0	0.0	–	–
16	328.8	318.85	716.9	0.05	0.0	–	–	–
17	512.2	502.25	1117.0	0.05	–	–	–	–
18	501.9	491.95	1093.0	–	–	–	–	–

(continued)

APPENDIX 6 (continued)

U234

Group	σ_{tr}	σ_{rem}	$\nu\sigma_f$	$\sigma_{g\to g+1}$	$\sigma_{g\to g+2}$	$\sigma_{g\to g+3}$	$\sigma_{g\to g+4}$	$\sigma_{g\to g+5}$
1	5.1	2.855	3.748	0.20	0.27	0.45	0.31	0.04
2	5.354	2.436	2.946	0.18	0.50	0.35	0.05	0.0
3	5.89	1.906	2.31	0.45	0.30	0.06	0.0	0.0
4	6.591	1.085	1.527	0,29	0.05	0.0	0,0	0.0
5	9.056	0,283	0.1817	0.05	0.0	0.0	0.0	0.0
6	12.713	0.589	0,0223	0.05	0.0	0.0	0.0	0.0
7	12.105	1.216	0.0	0.05	0.0	0.0	0.0	0.0
8	10.752	2.365	0.0	0.05	0.0	0.0	0.0	0.0
9	26.963	16.99	0.0	0.05	0.0	0.0	0.0	0.0
10	48.494	38.48	0.0	0.05	0.0	0.0	0.0	0.0
11	10.153	0.203	0.0	0.05	0.0	0.0	0.0	0.0
12	575.37	564.25	0.0	0.05	0,0	0,0	0,0	0.0
13	14.255	4.265	0.0	0.05	0.0	0.0	0.0	0.0
14	22.919	12.33	0.0	0.05	0.0	0.0	0,0	–
15	38.944	28.41	0.0	0.05	0.0	0.0	–	–
16	64.151	53.66	0.0	0.05	0.0	–	–	–
17	94.355	83.87	0.0	0.05	–	–	–	–
18	161.05	150.53	0.0	–	–	–	–	–

Aluminium

Group	σ_{tr}	σ_{rem}	$\sigma_{g\to g+1}$	$\sigma_{g\to g+2}$	$\sigma_{g\to g+3}$
1	1,929	0.808	0.642	0.120	0.030
2	2.322	0,634	0,380	0.220	0,034
3	2.344	0.578	0.395	0.170	0.012
4	2.896	0.264	0.264	0.0	0.0
5	3.519	0.188	0.188	0.0	0.0
6	2.921	0.123	0.123	0.0	0.0
7	1.458	0.06	0.06	0.0	0.0
8	1.410	0.05	0.05	0.0	0.0
9	1.410	0,05	0.05	0.0	0.0
10	1.460	0.10	0.10	0.0	0.0
11	1.470	0.11	0.10	0.0	0.0
12	1.490	0.12	0.10	0.0	0.0
13	1.510	0.13.	0.10	0.0	0.0
14	1.550	0,14	0.10	0.0	0.0
15	1.550	0.17	0.10	0.0	0.0
16	1.570	0.21	0.10	0,0	–
17	1.640	0.28	0.10	–	–
18	1.540	0.18	–	–	–

(continued)

APPENDIX 6 (continued)

Oxygen

Group	σ_{tr}	σ_{rem}	$\sigma_{g\rightarrow g+1}$
1	1.33	0.464	0.421
2	1.18	0.191	0.191
3	3.23	0.902	0.902
4	3.63	0.556	0.556
5	3.71	0.337	0.337
6	3.26	0.231	0.231
7	3.55	0.255	0.255
8	3.64	0.23	0.23
9	3.64	0.23	0.23
10	3.64	0.46	0.46
11	3.64	0.46	0.46
12	3.64	0.46	0.46
13	3.64	0.46	0.46
14	3.64	0.46	0.46
15	3.64	0.46	0.46
16	3.64	0.46	0.46
17	3.64	0.46	0.46
18	3.6412	0.0002	-

(b) 18–Group Fission Cross Sections used in Fission Ratio Calculations

Group	U233	U235	Pu239
1	1.75	1.21	1.90
2	1.83	1.22	1.95
3	1.89	1.22	1.83
4	1.94	1.20	1.70
5	2.24	1.43	1.67
6	3.23	2.50	2.04
7	5.98	4.22	3.04
8	8.96	7.95	4.06
9	23.9	17.59	15.2
10	53.0	60.05	10.1
11	101.6	58.47	88.1
12	89.6	24.3	33.5
13	288.8	24.8	21.9
14	131.5	61.9	147.0
15	182.5	166.7	1576.0
16	293.2	267.4	496.8
17	457.0	473.4	608.0
18	447.0	508.7	655.0

$\sigma_p = \infty$

APPENDIX 7

ENERGY SPECTRUM AT CENTRE OF CRITICAL SPHERE

Group	Lethargy Range (from 10 MeV)	Normalised Flux at Centre of Critical Sphere		
		Lattice I	Lattice II	Lattice III
1	1.204	5370	6670	7620
2	1.966	35669	43418	48942
3	2.408	40055	49499	56391
4	3.219	35812	44287	50483
5	4.605	43790	53826	61099
6	6.377	39447	48121	54342
7	8.0	40901	49504	55592
8	10.0	28980	34804	38870
9	12.0	28371	33758	37441
10	13.0	34979	41317	45565
11	14.0	34073	39893	43681
12	15.0	33109	38391	41702
13	16.0	31765	36250	38828
14	17.0	36914	41188	43378
15	18.0	70669	70738	69489
16	19.0	186681	159712	140064
17	19.8	188962	146002	117669
18	Thermal	84459	62624	48836

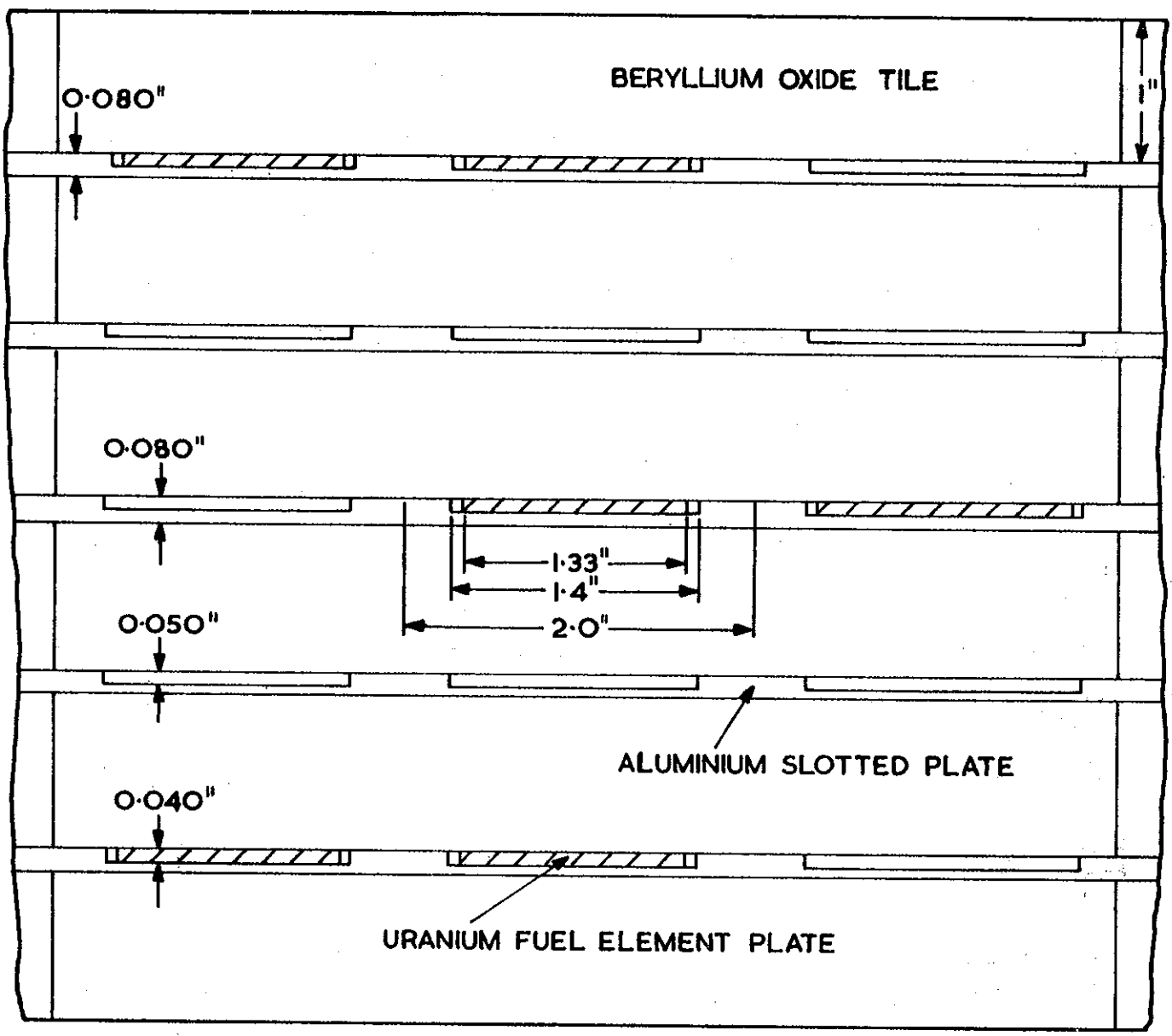

FIGURE 1 LATTICE I REPRESENTATIVE SECTION OF TOP FACE

P832

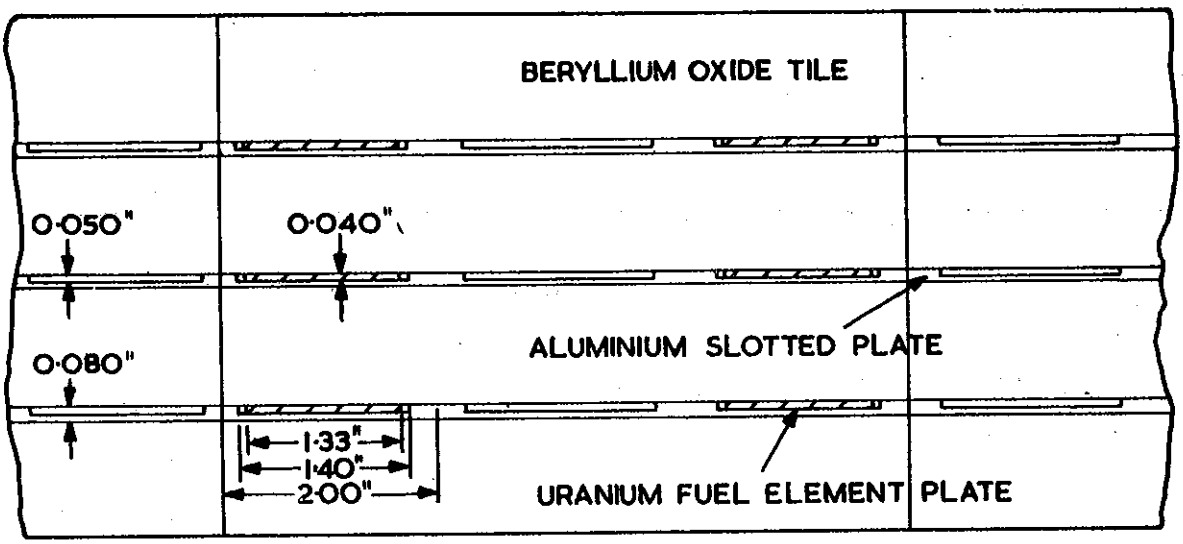

FIGURE 2 LATTICE II REPRESENTATIVE SECTION OF TOP FACE

P832

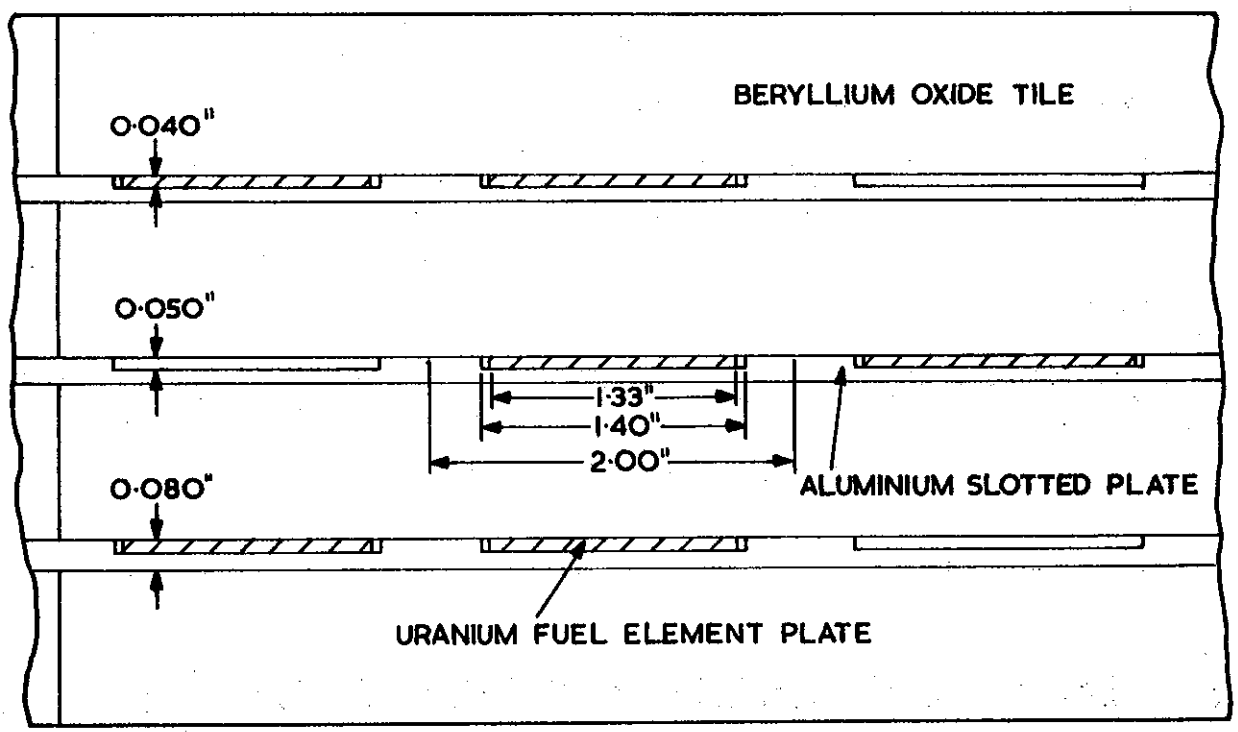

FIGURE 3 LATTICE III REPRESENTATIVE SECTION OF TOP PLATE

P832

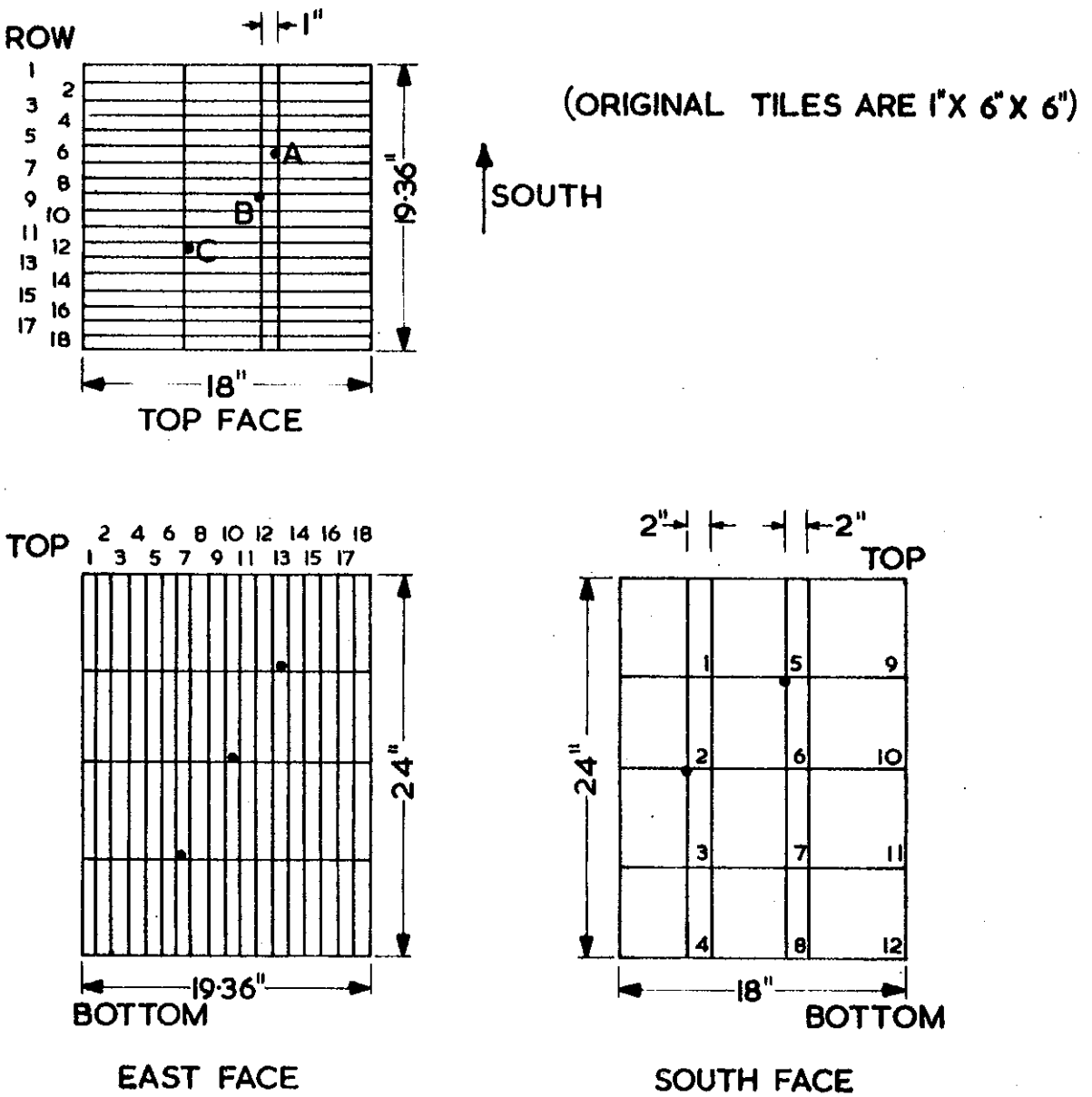

FIGURE 4 SCANNING HOLE POSITIONS

P832

LATTICE I

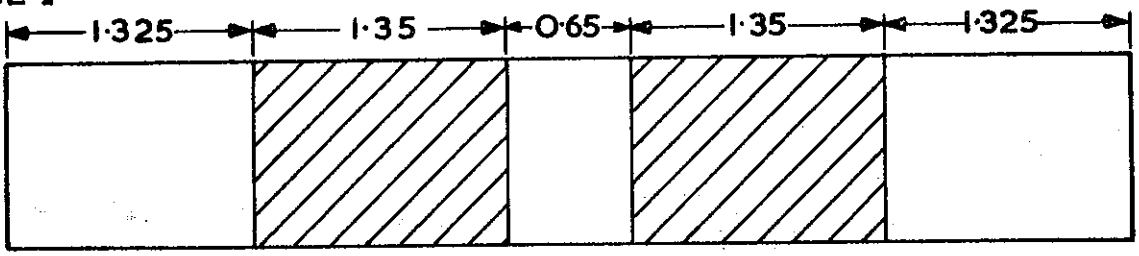

ATOMIC DENSITIES BeO 6·405 X 10^{22} ATOMS cm^{-3} THROUGHOUT
Al 2·944 X 10^{21} ATOMS cm^{-3} THROUGHOUT
U233 1·085 X 10^{19} IN SHADED REGIONS ONLY

LATTICE II

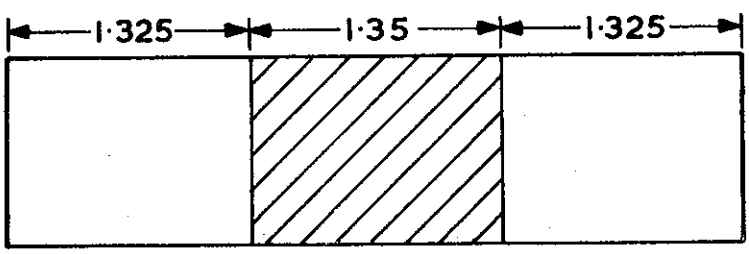

ATOMIC DENSITIES BeO 6·405 X 10^{22} ATOMS cm^{-3} THROUGHOUT
Al 3·163 X 10^{21} ATOMS cm^{-3} THROUGHOUT
U233 (SHADED AREA ONLY) 4·38 X 10^{19} ATOMS cm^{-3}

LATTICE III

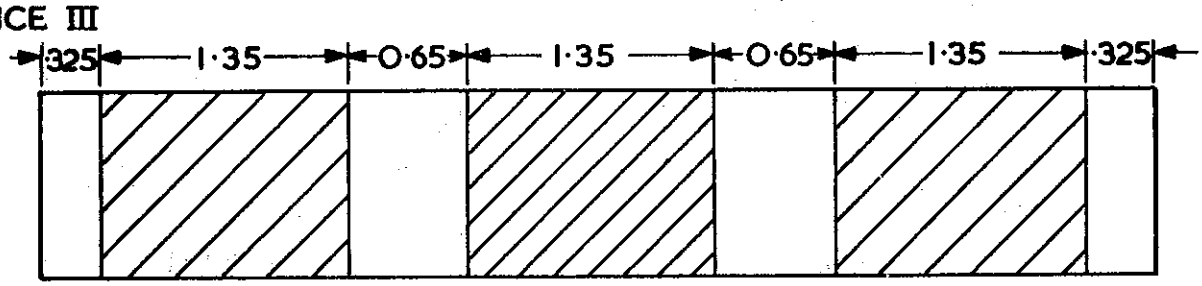

ATOMIC DENSITIES BeO 6·405 X 10^{22} ATOMS cm^{-3} THROUGHOUT
Al 3·382 X 10^{21} ATOMS cm^{-3} THROUGHOUT
U233 (CENTRE SHADED AREA) 4·38 X 10^{19} ATOMS cm^{-3}
(OUTER SHADED AREAS) 2·19 X 10^{19} ATOMS cm^{-3}

FIGURE 5 CELL STRUCTURE USED FOR DSN CALCULATIONS

P832

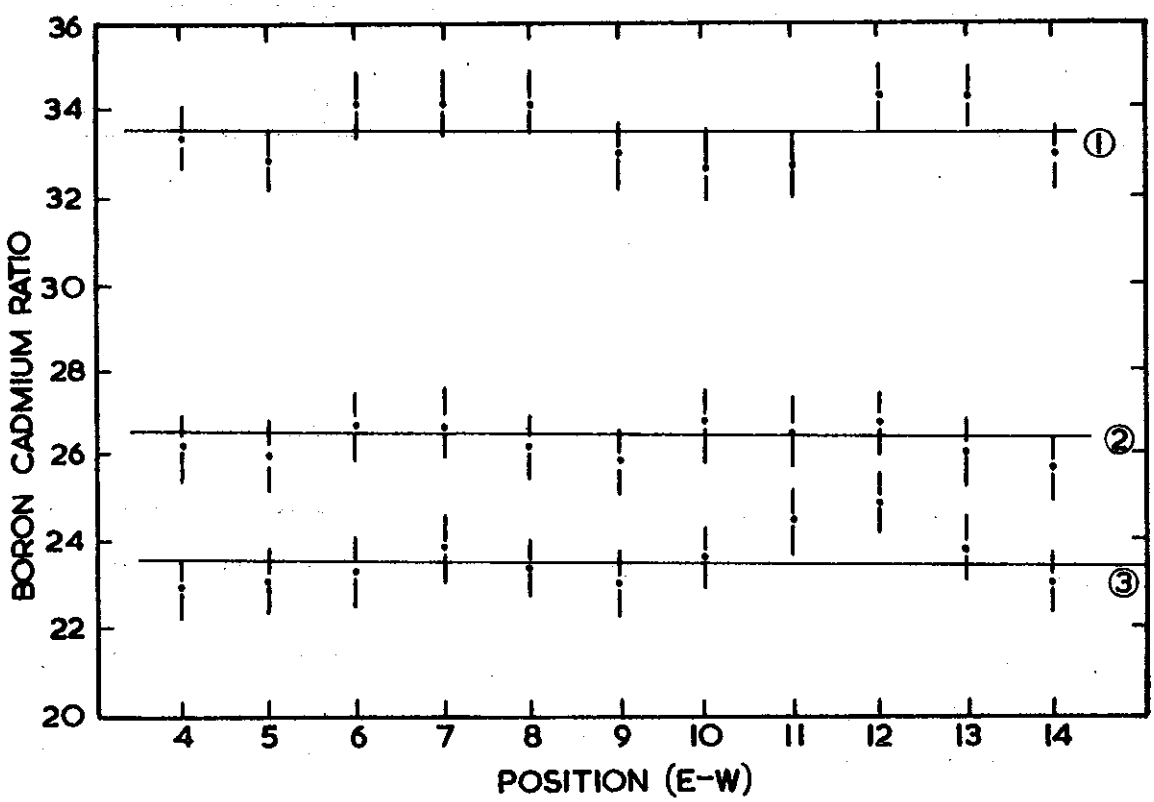

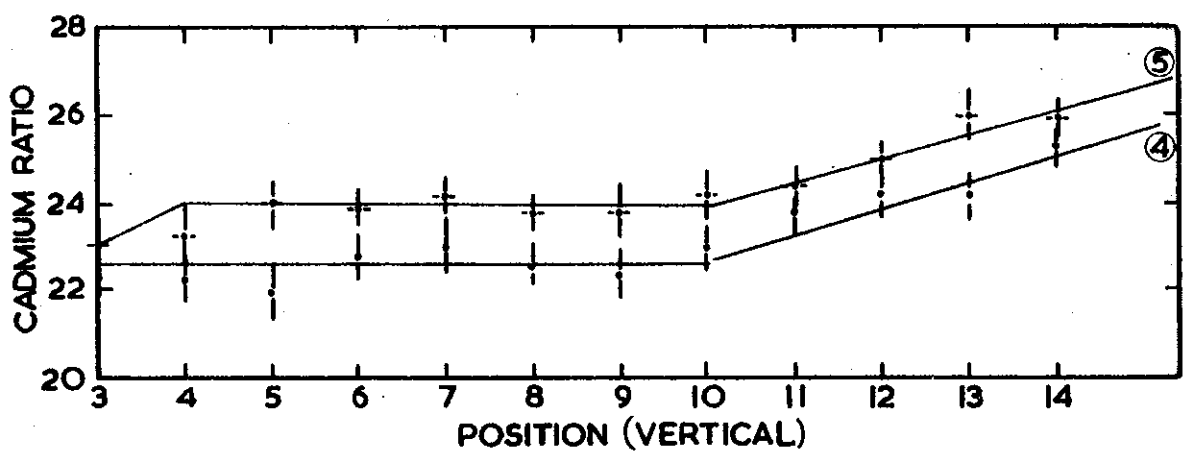

1 E-W 6" LEVEL (ALL POSITIONS USED)
2 E-W 12" LEVEL (ALL POSITIONS USED)
3 E-W 18" LEVEL (ALL POSITIONS USED)
4 VERTICAL HOLE B (POSITIONS 4-10 USED)
5 VERTICAL HOLE C (POSITIONS 4-10 USED)

FIGURE 6 CADMIUM RATIOS LATTICE I

P032

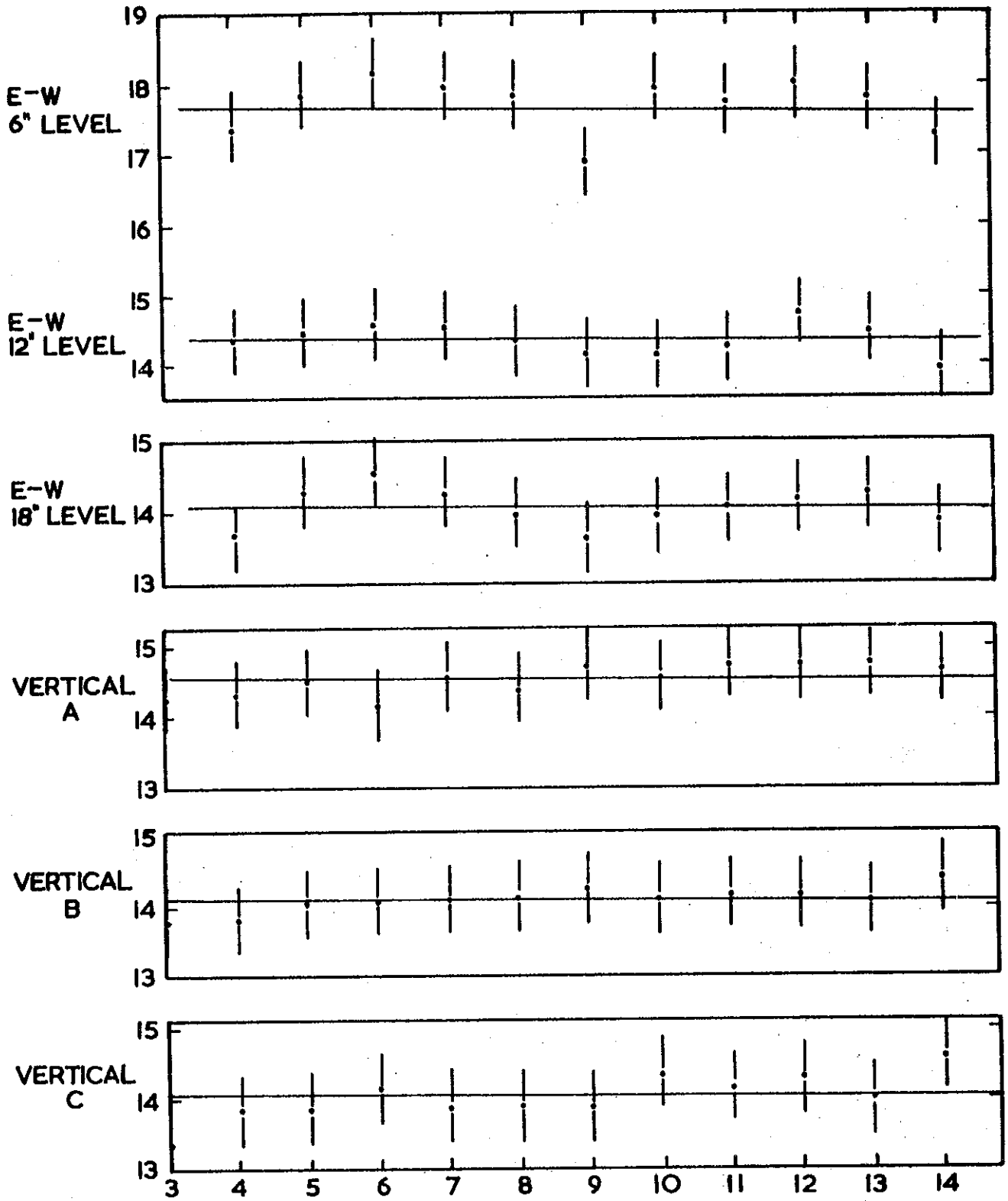

FIGURE 7 CADMIUM RATIO PLOTS LATTICE III

P832

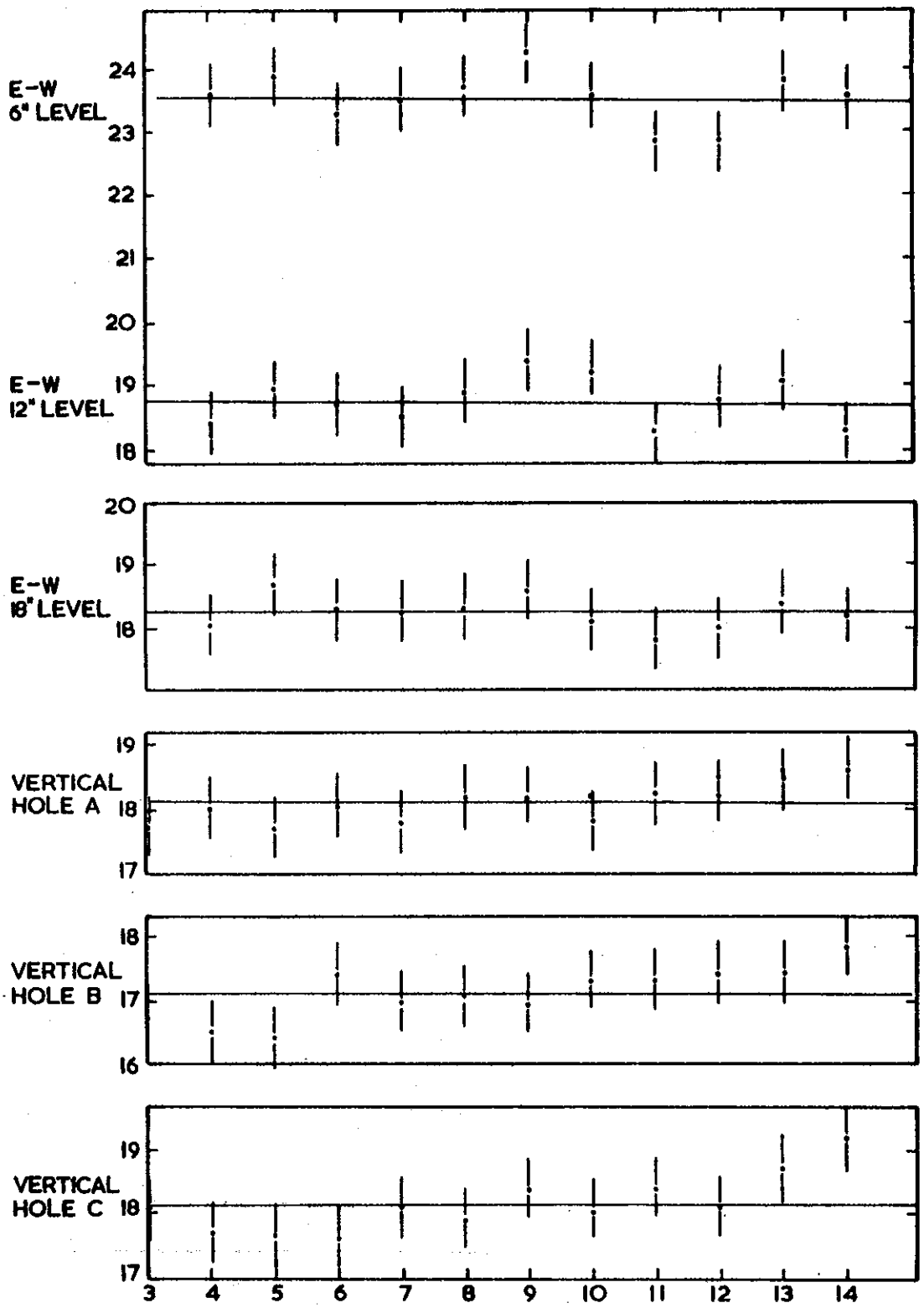

FIGURE 8 CADMIUM RATIO PLOTS LATTICE II

P832

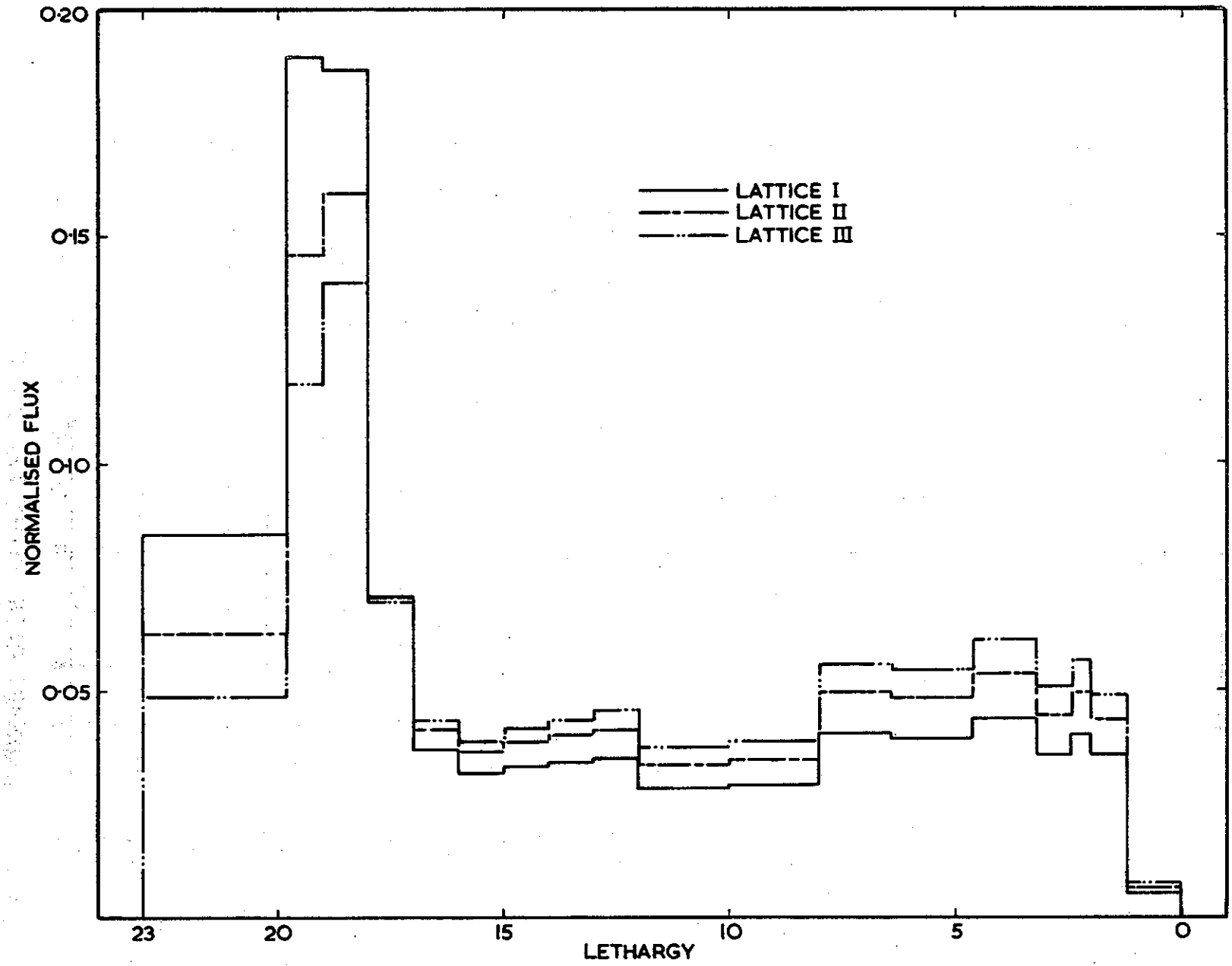

FIGURE 9 NORMALISED FLUX PER UNIT LETHARGY INTERVAL

P832

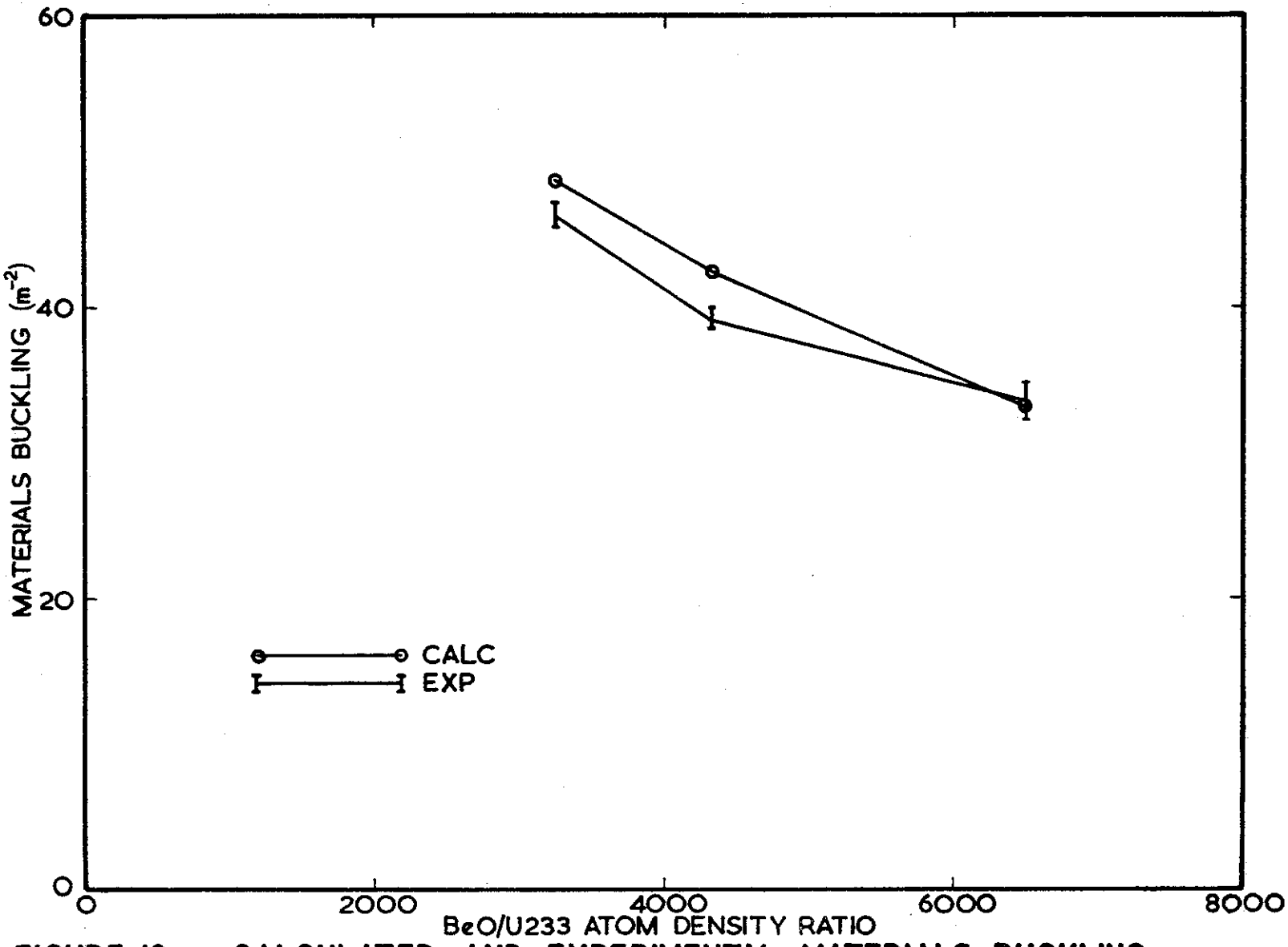

FIGURE 10 CALCULATED AND EXPERIMENTAL MATERIALS BUCKLING

P832

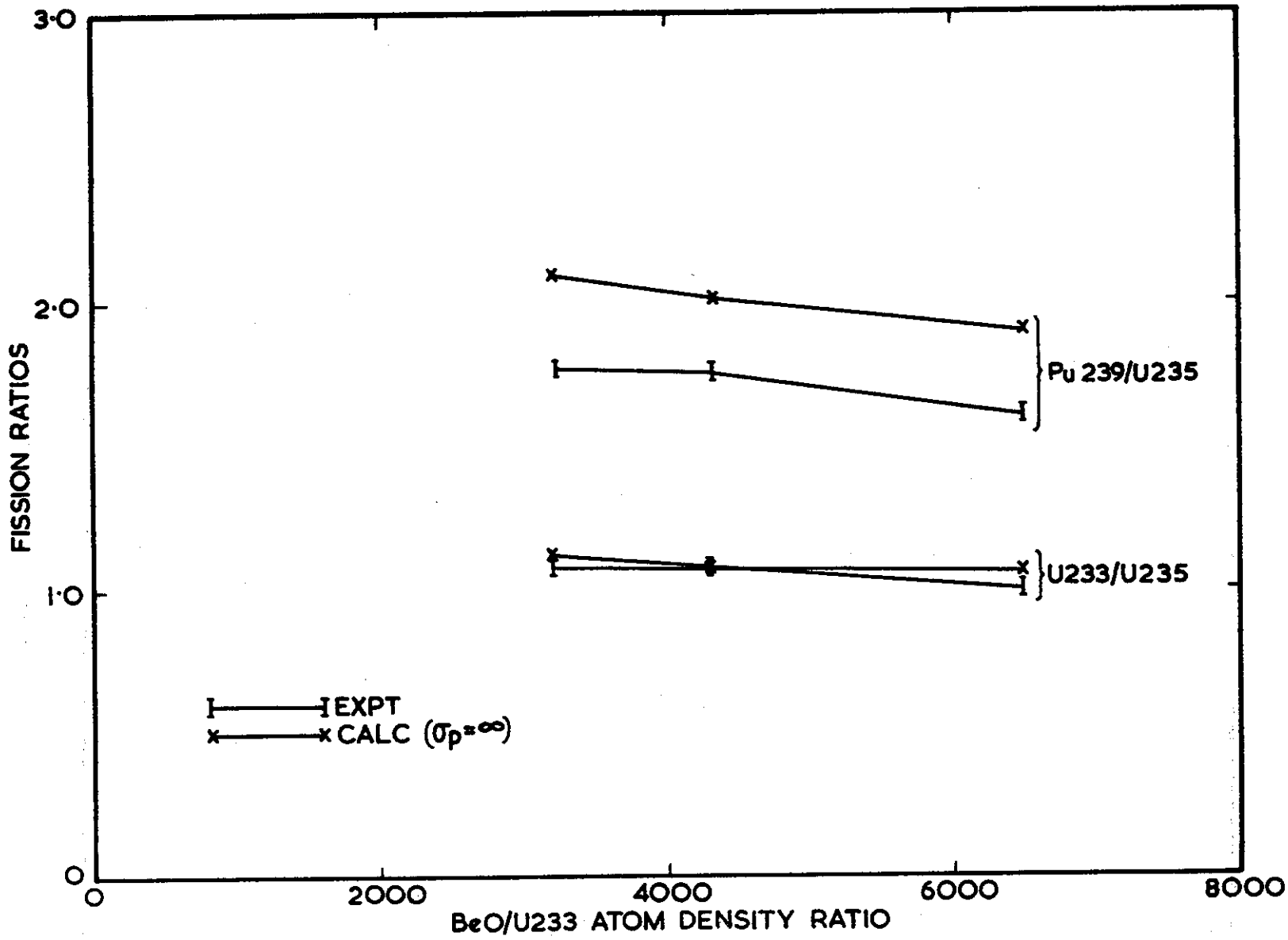

FIGURE 11 CALCULATED AND EXPERIMENTAL FISSION RATIOS

P832